Modelling of friction stir welding of 304 stainless steel

SMITH, Alan <http://orcid.org/0000-0001-7868-8501>, AL-MOUSSAWI, M., YOUNG, Andrew E, CATER, S. and FARAJI, M.

MODELLING OF FRICTION STIR WELDING OF 304 STAINLESS STEEL

*Smith A.
*¹ Al-moussawi M.
*Young A.
*Sheffield Hallam University/MERI/UK
*¹b1045691@my.shu.ac.uk

Cater S.
TWI/South Yorkshire/UK

Faraji M.
Coventry University /UK.

KEYWORDS

Friction Stir Welding, Computational Fluid Dynamics, 304 Stainless steel.

ABSTRACT

A 3-D Eulerian steady-state CFD model has been developed to simulate the Friction Stir Welding (FSW) of 6mm plate 304 stainless steel (304SS). The Polycrystalline BoroNitride- Tungsten Rhenium (PCBN-WRe) hybrid tool was modelled with the workpiece in a fully sticking condition. The viscosity of stainless steel was calculated from the flow stress equation taken from a previous study of hot working carried out in a range of temperatures between 800°C-1200 ^{o}C and strain rates 0.001 s^{-1} to 5 s^{-1}. The model predicted the temperature distribution in the Stirred Zone (SZ) for three welding cases including low, intermediate and high rotational speed/traverse speeds. The model also predicts that localised melting may occur if the tool rotational speed exceeds 400RPM. Finally, the model suggested a larger probe (12mm diameter at the shoulder base and 5.8mm length) with a stationary shoulder would prevent the localised melting and allow an increase in welding speeds without the associated introduction of stagnant zone related weld defects.

1-INTRODUCTION

Friction Stir Welding (FSW) was invented by TWI/UK in 1991 and is predominantly applied to low melting alloys such as aluminium and magnesium. The challenge of welding higher melting point alloys, such as steel, is closely allied to the requisite working temperature and pressure and therefore the associated cost of the tool (Toumpis et. al. 2015). This problem is exacerbated if the steel to be welded has a low thermal conductivity, as would be the case when FSW an austenitic stainless. This is because the low thermal conductivity increases the probability of localised melting during the FSW process. Modelling of the FSW process can help to inform the selection of suitable welding parameters particularly the rotational and traverse speeds of the tool thus reducing the time and effort expended on numerous "trial and error" experiments. However, modelling can also be a challenge because of the complexity associated with the FSW process which includes high strain rate, material flow, heat generation and partitioning at the tool/workpiece interface. Modelling of FSW is possible using Computational Fluid

Dynamics (CFD) in which the material flow, viscosity and strain rate are represented effectively. There have been few attempts at modelling FSW of high melting, low thermal conductivity alloys such as 304 Stainless Steel (SS). (Pal and Phaniraj 2015) produced a three dimensional CFD modelling to simulate the FSW of 304SS. They calculated the heat partition between the Poly Crystalline Boron Nitride (PCBN) tool and workpiece and found that 81% of the total heat generated in the tool/workpiece interface was transferred to the workpiece. The tool's shoulder/workpiece interface was found to experience the maximum temperature gradient. The result from the temperature distribution model was validated against previous experimental work on 304SS. Their model also predicted defects related to the formation of a stagnant zone on the advancing side of the tool, Figure 1. (Elbanhawy et al. 2013) also applied a CFD model in an Eulerian framework to simulate the FSW of a grade 304 stainless steel using a PCBN hybrid tool. Two types of viscosity equation were used, linear and non-linear non-Newtonian fluid. Viscose heating represented the main source of heat generated in the tool/workpiece interface. They found that the model identified small molten regions when the welding traverse speed exceeded 150 mm/min and the rotational speed exceeded 250RPM. (Darvazi and Iranmansh 2014) applied a finite element thermal model on FSW of (304SS) and represented the heat generated as originating from plastic and frictional sources. Their model predicted a temperature of 1000°C at the tool/shoulder interface when the tool rotational and traverse speeds were 300RPM and 80mm/min respectively. Although their model represented the asymmetry between advancing and retreating sides, it did not predict any local melting at these velocities. In this paper the FSW of 304SS was modelled using the CFD technique and the FLUENT software. The welding and traverse speeds were chosen as low 200 RPM/125mm/min, intermediate 250 RPM/ 200mm/min and high 350 RPM/300mm/min. Another high welding speed of 400 RPM/400mm/min was included in an attempt to establish the limits of welding speed that can cause the onset of localised melting. Viscosity was calculated from previous hot work on 304SS and represented in the model as a User Defined Function (UDF). The results of temperature distribution were compared and validated against previous numerical and experimental published work. The model predicted an asymmetry in temperature between the advancing and retreating sides and also the size of the stirred zone based on the results of the viscosity contours.

2-MATERIALS AND NUMERICAL METHOD:

2-1 Materials of the Workpiece and Tool: The chemical composition of 304LSS is as shown in Table 1(Nkhoma et al. 2014), thermal properties for the workpiece (304L SS) is shown as (AK steel Ltd): $k = Thermal\ Conductivity = 16.2\frac{W}{m.K}$ T<100°C, $Cp = Specific\ heat\ capacity = 500\frac{J}{Kg.K}$, $\rho = Density$=8003$\frac{Kg}{m^3}$

Table 1: The chemical composition of 304 SS grade

304 SS Chemical Composition wt.%					
C	Si	Mn	P	S	Al
0.024	0.38	1.43	0.027	0.0023	0.003
Cr	Ti	Cu	Co	N	Ni
18.2	0.001	0.15	0.07	0.072	8.1

The FSW tool of PCBN-WRe with a shoulder radius of 12.5mm and a pin base radius of 5mm with a pin base length of 5.5mm l. The PCBN tool as shown in Fig. 1 is hybrid and includes a shank made of WC and both the PCBN and shank are surrounded by a collar made of Ni-Cr. The thermal properties for the PCBN hybrid tool are as in the previous published work (Almoussawi et al. 2016)

2-2 The Tool and Plate Geometries and the CFD Model Assumptions. The surface of the tool parts were designed in Pro-Engineer software and then converted to ANSYS-Fluent. The total dimensions of the plate used for experimental verification work were not modelled because of the low thermal conductivity and the small HAZ expected in stainless steel. So the plate was designed as shown in Figure 1 with a dimension of 300mm long × 200mm wide × 6mm thick. The tool and plate were assumed to be in direct contact.. The backing plate was not represented but a thermal convection with a high value (2000 W/m².K) was applied to the bottom surface of the plate (Micallef et. al. 2015), this is also to increase the computation efficiency.
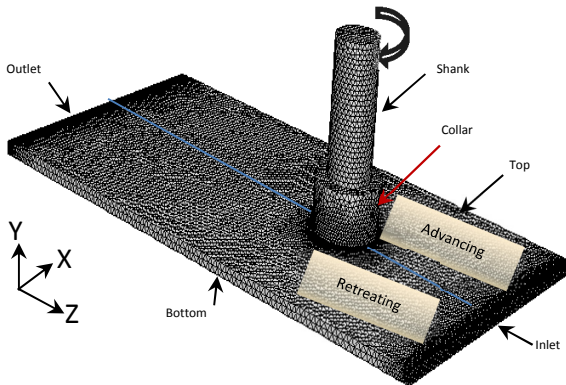

Figure 1: a- Geometry, boundary conditions and mesh.

CFD Model assumption: Assumptions which used in the model shown in Figure 1 were taken from previous work for the authors (Al-moussawi et al. 2016) but with two differences. Firstly, the heat generated will mainly be from viscose heating (velocity gradient and viscosity $\mu(\nabla^2 u)$) and secondly fully sticking conditions between the tool and workpiece were applied.

2.3 The Governing Mathematical Equations:

Below is the summary of mathematical equations applied in the model: As the material under investigation is incompressible, the continuity equation can be represented as: (Nandan et. al. 2007)

$$\frac{\partial u_i}{\partial x_i} = 0 \tag{1}$$

u_i-is the velocity of plastic flow in index notation for i=1, 2 and 3 which representing the Cartesian coordinate of x,y and z respectively. The temperature and velocity fields are solved assuming steady state behaviour. The plastic flow in a three dimensional Cartesian coordinate system can be represented by the momentum conservation equation in index notation with i and j=1,2 and 3, representing x,y and z respectively (Nandan et. al. 2007)

$$\rho\frac{\partial u_i u_j}{\partial x_i} = -\frac{\partial p}{\partial x_j} + \frac{\partial}{\partial x_i}\left(\mu_u\frac{\partial u_j}{\partial x_i} + \mu_u\frac{\partial u_i}{\partial x_j}\right) - \rho U\frac{\partial u_j}{\partial x_1} \tag{2}$$

ρ=density (Kg/m³), p=pressure Pa , U=welding velocity m/sec, μ_u=Non-Newtonian viscosity Pa.s. Viscosity is equal to the flow stress divided by the effective strain rate (Nandan et. al. 2007):

$$\mu_u = \frac{\sigma_f}{3\varepsilon^.} \tag{3}$$

Maximum stresses is normally determined from a Sin-hyperbolic (Sinh) constitutive equation. The flow stress (perfectly plastic model) proposed by Sheppard and Wright (Nandan et. al. 2006) is:

$$\sigma_f = \frac{1}{\alpha}sinh^{-1}[(\frac{Z}{Ai})^{\frac{1}{n}}] \tag{4}$$

Where n, Ai, α are material constants taken from previous work carried on 304L stainless steel (Nkhoma et al. 2014) (A_i=1.2 x10^{17} MPa^{-1}.s^{-1} , α=0.008 , n=6.1). Z_n is the Zener-Holloman parameter which represents the temperature compensated effective strain rate as (Nandan et. al. 2006):

$$Zn = \varepsilon^.\exp\left(\frac{Qe}{RT}\right) = Ai[\sinh\alpha\,\sigma_f\,)]^n \tag{5}$$

Qe-is the activation energy and equal 446000 J/mole (Nkhoma et al. 2014), R is the gas constant. The effective strain rate can be represented as (Nandan et. al. 2007):

$$\varepsilon^. = \sqrt{\frac{2}{3}\varepsilon_{ij}\varepsilon_{ij}} \tag{6}$$

ε_{ij}- is the strain tensor which can be represented as:

$$\varepsilon_{ij} = \frac{1}{2}\left(\frac{\partial u_j}{\partial x_i} + \frac{\partial u_i}{\partial x_j}\right) \tag{7}$$

2.4 Heat Equations: The material flowing through the mesh in a Eulerian steady state solution (Schmidt and Hattel 2006):

$$\rho C_p \nabla(uT) = \nabla(k \nabla T) - \rho C_p v_x \frac{\partial T}{\partial x} + Q_i + Q_b \quad (8)$$

k=Thermal conductivity in (W/m.K) , C_p= Specific Heat (J/Kg. K), v_x =Velocity in the X-direction, T= Temperature. Q_i = Heat generated due to tool/workpiece interface and here is mainly represented from the viscous shear forces and calculated as $(\mu_u \nabla^2 u)$. Q_b = Heat generated due to plastic deformation away from the interface and is ignored in this work because of insignificant contribution to heat generation (Nandan et al. 2007).

2.5 CFD Model Boundary Conditions

A- Representing the Material Flow velocity.

The velocities (u,w) in the x and z directions can be obtained as below. Velocity in the normal Y direction was not represented because of the fully sticking assumption.

$$u = (1 - \delta)(\omega r \sin\theta - U) \quad (9)$$

$$w = (1 - \delta)(\omega r \cos\theta) \quad (10)$$

B-Heat Fraction Generated Between the Tool and the Workpiece: Due to the low thermal conductivity of 304SS compared to the PCBN tool which is about five times that of 304SS, most of the heat generated in the FSW process will be fractioned between the tool and work piece. Other researchers (Darvazi et. al. 2014) (Nandan et. al. 2007) calculated this fraction (*f*) as:

$$f = \frac{J_{WP}}{J_{WP} + J_{TL}} = \frac{\sqrt{(k\rho C_p)_{WP}}}{\sqrt{(k\rho C_p)_{WP}} + \sqrt{(k\rho C_p)_{TL}}} \quad (11)$$

$$q = h(T - T_\circ) + \epsilon\sigma(T^4 - T_\circ^4) \quad (12)$$

Where: *f* =Heat Fraction between the tool and workpiece, ϵ =Emissivity of the Plate Surface, β is Stefan-Boltzmann constant $(5.670373(21) \times 10^{-8}$ W m^{-2} K^{-4}). T_o= Initial temperature ^{o}C, h= Thermal Convection Coefficient (W/m^2.^{o}C).The abbreviation WP and TL refer to the workpiece and the tool respectively. For FSW using a PCBN tool with a cooling system, as in this work, the equation cannot accurately represent the fraction of heat distribution between tool and workpiece so it is more appropriate to represent the tool within the model geometry [Almoussawi et al. 2016].

C-Heat Losses from the Workpiece Surfaces (Top and Sides): Convection and radiation in heat transfer are responsible for heat loss (*Q*) to the surroundings as represented by Eq (2). In the current model radiation will not be calculated as it will also add more complexity to the case. Instead the value of heat lost by radiation was considered by increasing the value of the heat convection coefficient around the tool. (Micallef et. al. 2015).

D-Heat Loss from the Workpiece Bottom Surface: The bottom of the workpiece is in direct contact with two other plates (usually mild and O_1 steel grades) and the anvil. Previous workers (Khandkar et. al. 2003) (Micallef et. al. 2015) have suggested representing the backing plates effects by a convection heat condition with a high coefficient of heat transfer value (500-2000 W/m^2. ^{o}C). A value of 2000 W/m^2. K was used which gave a reasonable agreement to the temperature distribution reported from previous published work. The initial temperature of the workpiece was set to room temperature (25°C). All governing equations and boundary conditions were carried out in Fluent software which is capable of solving the 3D equations of velocity and momentum.

Table 2: Welding Conditions used in the CFD Model.

| Weld No.	Rotational speed ω RPM	Traverse speed V mm/min	ω/ V rev/mm	Torque N.m
W1	200	125	1.6	117
W2	250	200	1.25	102
W3	300	350	0.857	90
W4	400	400	1	67

3- RESULTS AND DISCUSSION:

3.1 Temperature Contours: The contours of temperatures distribution around the FSW tool for simulated welding conditions W1 to W4 are shown in Figure 2. Note how the temperature in the tool/workpiece contact surface is very high and the contours tend to expand towards the trailing side. The contours also tend to be more compressed when the traverse speed increase as in the cases of W3 and W4 and thus the cooling rate is expected to increase. The temperature also showed asymmetry between the advancing and retreating sides with a maximum temperature at the advancing-trailing side. The asymmetry is increased in W3 and W4 as the tool speeds increase. These results coincide with the previous finding of (Fehrenbacher et al. 2014) in which they showed experimentally that the maximum temperature is on the advancing trailing side. (Darvazi et al. 2014) found from numerical modelling that the maximum temperature of FSW 304SS is located at the back of the tool but near the advancing side. (Micallef et al. 2015) also found that the maximum temperature, which was validated experimentally by thermocouples, is always at the advancing-trailing side. It was assumed that this maximum temperature was associated with the maximum plastic deformation caused by the low viscosity on the advancing-trailing side. The maximum temperature of W1 shown in Figure 2 was 1123°C which is close to the temperature measured experimentally at TWI for the same steel grade and welding conditions (Elbanhawy et al. 2013).
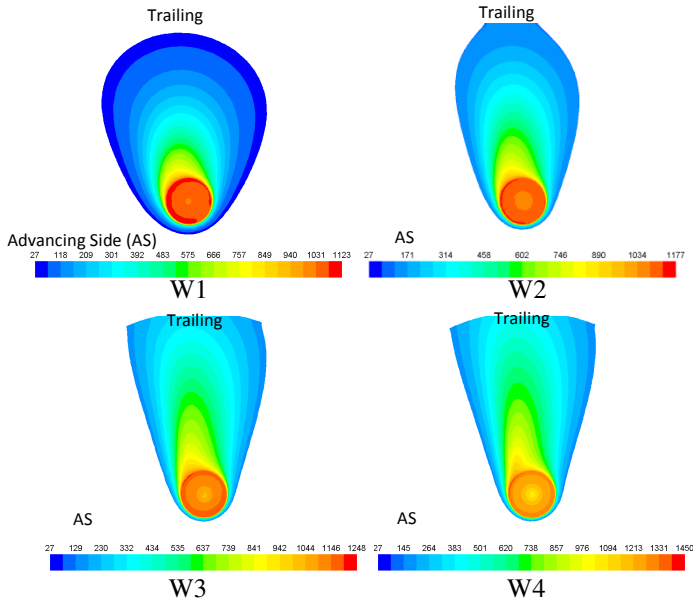
Figure 2: Contours of temperatures (°C), Top view of the tool/workpiece contact region.

The estimated torque calculated during the CFD solution was 117 N.m which is also in close agreement with the experimental value measured by (Elbanhawy et al. 2013) from the FSW machine (112 N.m). These results can give some confidence regarding the assumptions made in arriving at the current model and the results from it. The temperatures generated in W1 to W4 is at a maximum under the tool shoulder and increases with the tool rotational speed despite the increase in tool travelling speed as shown in Table 3. These findings suggest that tool rotational speed is the main contribution to the heat generated, whereas, the travel speed appears to have greater influence over the cooling rate. W4 shows that the temperature under the shoulder of the tool is close to the melting point of the parent material (1400 °C to 1450°C) so, based on this model it would be recommended to perform the FSW process for 304SS using PCBN hybrid tool under a rotational speed below 400RPM and at a travel speed of 400mm/min . However, by optimising the tool's design which includes a stationary shoulder and slightly bigger probe as will be discussed later, the welding could be carried out using faster welding speeds.
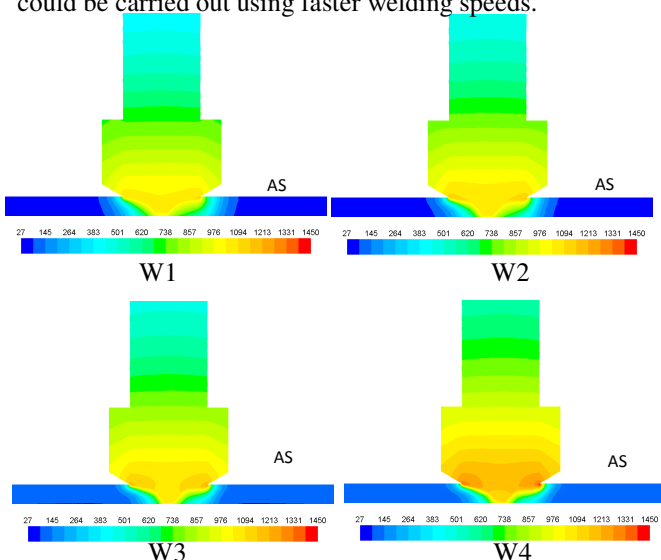
Figure 3: Contours of temperatures (°C), Normal section to the welding direction.

Figure 3 is a normal section to the welding direction and represents the temperature distribution between the advancing and retreating sides. The Heat Affected Zone (HAZ) as expected is very small compared to the geometry size of the work piece; which is due the low thermal conductivity of 304 SS. The HAZ is bigger in the case of low welding speeds as in W1 because of higher heat input generated in the workpiece at lower traverse speed as expected. This is in accordance with the numerical modelling of (Micallef et al. 2015) which showed that the HAZ size is increased as the travelling speed decreases. (Colegrove and Shercliff 2005) also showed that the HAZ increases as the tool rotational speed increases and the traverse speed decrease. The asymmetry in temperature between the advancing and retreating sides also increases and is shown in case of W3 and W4; this can be related to the velocity and strain rate which is higher at the advancing side as more material is pushed towards the advancing trailing side. This will be discussed later in this paper. It is also shown in Figure 3 for all cases under study that the temperature contours of the tool are circulated toward the tool shank; this is because of the fact that low thermal conductivity of the tool collar is acting as an insulator so most of the heat is partitioned between the PCBN-shank and the workpiece.

3.2 Viscosity in the Stirred Zone (SZ): The viscosity contours shown in Figure 4 are representing the total stirred zone (SZ) affected by the tool rotation and traverse speeds. It should be noted that the viscosity decreases significantly with increasing tool speeds; this is related to the increase in temperature and strain rate. Towards the probe end there appears to be an increase in viscosity which is most likely related to the decrease in material circulation which, in turn, leads to a decrease in temperture and strain rate. This mechanism may be the reason for the V-shaped geometry usually found in the SZ. (Nandan et al. 2007) found the same decrease in viscosity towards the probe end. It can also be shown that the most affected zone by tool stirring is located between the tool shoulder and probe side due to the combination effect of these two mechanisms.
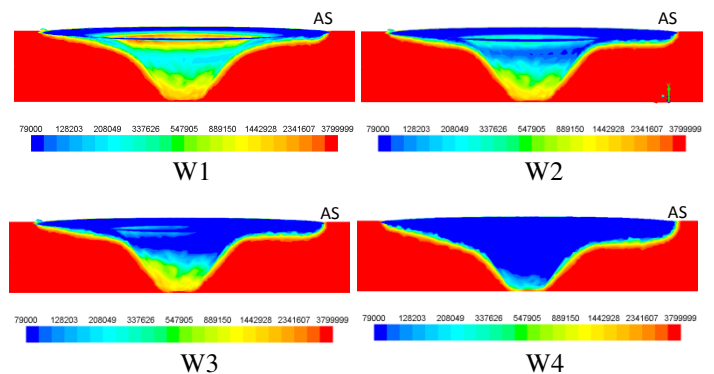
Figure 4: Viscosity Distribution in the Stirred Zone (SZ) for W1-W4, (Normal section to the welding direction).

3.3 FSW Tool Design Optimisation: An optimisation has been carried out on the tool geometry in order to make the FSW of 304SS more robust and prevent the localised melting which may occur at high welding speed. A stationary shoulder with probe length of 5.8mm and a

probe diameter of 12mm at the shoulder base and 5mm at the probe end appears to be suitable for higher welding speeds. Figure 5 shows the CFD model results, based on this optimised tool design, for temperature, strain rate, velocity and viscosity at welding speeds of 550RPM and 400 mm/min. It is assumed that the tool probe is fully plunged into the workpiece and the tool shoulder is in contact with the top surface of the plate. The maximum calculated temperature was $1065^{o}C$ which is below the melting point of a grade 304 stainless steel and it also shows less asymmetry between the advancing and retreating sides. The distribution of the strain rate, velocity and viscosity in the middle of the probe is almost uniform except at the top where the material circulation is higher and at the probe end where the circulation is reaching the lowest value.

a-Temperature distribution ^{o}C b-Strain rate s^{-1}

c-Velocity m/s   d-Viscosity Pa.s
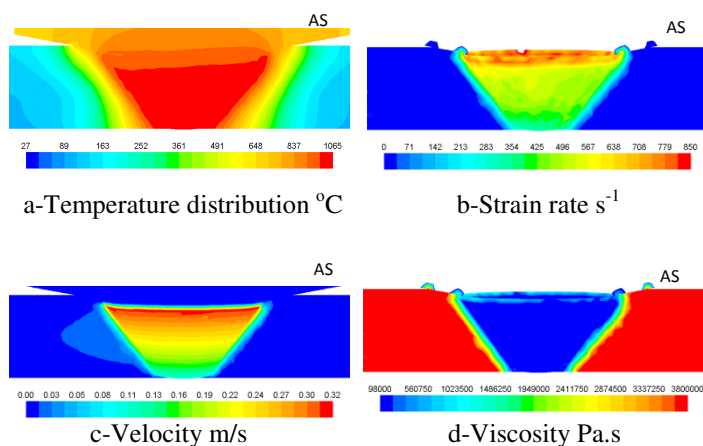
Figure 5: The results of CFD model of the optimised FSW tool design presented in terms of (a)-temperature ^{o}C, (b)-strain rate s^{-1}, (c)-velocity m/s and (d)-viscosity. Welding rotational speed 550RPM and traverse speed 400mm/min.

CONCLUSION:

From the results and discussion the it can be concluded that, the proposed CFD model predicts that, under the conditions of modelling, friction stir welding of a grade 304 stainless steel can be performed over a limited range of tool rotational speeds and traverse velocities. The high rotational speed and low thermal conductivity is reason for local melting problem at high rotational speed. The proposed CFD model predicts that if excessive FSW tool rotational speeds (in excess 400RPM) are used the localised melting of the parent material (grade 304) will occur. A new design of PCBN-WRe tool which employs a stationary shoulder and a larger probe can solve the issues of localised melting of the parent material at high tool rotational speeds. This also can reduce the tool cost which is the main obstacle for greater integration of FSW of stainless steel.

FUTURE RESEARCH

Investigating the defects formation and material flow especially at high welding traverse speed.

REFERENCES

Almoussawi A., Smith A, Andrew Y, Cater S., Faraji M, 2016, " An Advanced Model of Friction Stir Welding of DH36 Steel", 11th International Symposium of Friction Stir Welding, Cambridge, UK.

Colegrove P and Shercliff, 2005, "3-Dimensional CFD modelling of flow round a threaded friction stir welding tool profile", H., Journal of Materials Processing Technology, 169, 320–327

Darvazi, A.R. & Iranmanesh, M., 2014, "Thermal modeling of friction stir welding of stainless steel 304L. The International Journal of Advanced Manufacturing Technology",75 (9-12), pp.1299–1307.

Elbanhawy A., Chevallier E., Domin K., 2013, "Numerical investigation of friction stir welding of high temperature materials", NAFEMS world congress, Salzburg, Austria, 9-12 June 2013.

Khandkar, M.Z.H., Khan, J. A. & Reynolds, A. P., 2003. "Prediction of temperature distribution and thermal history during friction stir welding: input torque based model", Science and Technology of Welding and Joining, 8(3), pp.165–174.

Micallef, D., Camilleri, D., Toumpis, A., Galloway, A., & Arbaoui, L. (2015). "Local heat generation and material flow in friction stir welding of mild steel assemblies". J Materials: Design and Applications, 230 (2), pp. 586-602.

Nandan R. , Roy G.G. , Lienert T.J., Debroy T., 2007. "Three-dimensional heat and material flow during friction stir welding of mild steel". Acta Materialia, 55(3), pp.883–895.

Nandan, R., Roy, G.G. , Debroy, T., 2006. "Numerical Simulation of Three-Dimensional Heat Transfer and Plastic Flow During Friction Stir Welding". Metallurgical and materials transaction A , 37A, pp1247-i

Nkhoma Richard K.C., Siyasiya Charles W., Stumpf Waldo E., 2014, "Hot workability of AISI 321 and AISI 304 austenitic stainless steels", Journal of Alloys and Compounds 595 (2014) 103–112.

Pal Subrata, Phaniraj M.P., 2015, "Determination of heat partition between tool and workpiece during FSW of SS304 using 3D CFD modelling", Journal of Materials Processing Technology, (222), pp. 280–286.

Schmidt H.N.B., Dickerson T.L., Hattel J.H., (2006), "Material flow in butt friction stir welds in AA2024-T3". Acta Mater. 54, pp. 1199–1209.

WEB REFERENCES

AK Steel, http: // www. aksteel. com/pdf/ markets_ products /stainless/austenitic/304_304l_data_sheet.pdf